Electrical Power and Energy Systems 119 (2020) 105939

Contents lists available at ScienceDirect

Electrical Power and Energy Systems

journal homepage: www.elsevier.com/locate/ijepes

An enhanced sub-cycle statistical algorithm for inrush and fault currents classification in differential protection schemes

Mohsen Tajdinian[a], Mehdi Allahbakhshi[a], Alireza Bagheri[a], Haidar Samet[a], Payman Dehghanian[b,*], Om Parkash Malik[c]

[a] Department of Power and Control Engineering, School of Electrical and Computer Engineering, Shiraz University, Shiraz, Iran
[b] Department of Electrical and Computer Engineering, George Washington University, Washington, DC 20052, USA
[c] Department of Electrical and Computer Engineering, University of Calgary, Calgary, AB T2N 1N4, Canada

A B S T R A C T

Differential protection is a widely-used approach for power transformer protection, the performance of which may be, at times, challenged due to the inrush current and current transformer (CT) saturation. This paper presents an enhanced statistical algorithm for discrimination of fault and inrush current signals under CT saturation scenarios. This paper proposes twofold discrimination indices centered on the concept of fourth-order statistic moment, the so-called kurtosis on the current signal. Mathematically proven, the algorithm performance only depends on the current signal phase angle and it does not require transformer parameters. The mathematical closed form formulation in this paper classifies fault condition and inrush currents in sub-cycle timeframes even in the CT saturation conditions. The performance of the proposed algorithm is verified under various fault and inrush current scenarios with and without CT saturation. The numerical results demonstrate that the proposed algorithm can successfully classify the disturbances and detects saturations quickly with promising accuracy.

Index Terms: Inrush current; internal fault; current transformer saturation; differential protection

1. Introduction

Differential protection unit on a power transformer is one most significant protection scheme against failures due to internal faults. Since differential relays typically operate under conditions where considerable differential currents exist, inrush currents may potentially cause mal-operation of differential relays [1,2]. As a result, fast, accurate and reliable discrimination between internal fault conditions and inrush currents helps preventing the false trips of the differential relays.

Surveying the related literature, there exist two main types of algorithms in such applications: (i) algorithms for current transformer (CT) saturation detection which may also work on waveform reconstruction, and (ii) algorithms to distinguish between internal faults and inrush currents. In the first category, almost all the state-of-the-art methods are able to detect CT saturation only if they are fed by a standard fault signal [3]. Such methods range from model based algorithms [4–12], artificial intelligence based algorithms [13–15], and hybrid signal processing algorithms [3,16–18]. Except in [3] and [6], most CT saturation detection and waveform reconstruction algorithms are not able to distinguish inrush currents which potentially imposes a risk to the accurate operation of the protection functions. This is particularly critical as CT saturation may be more frequently experienced in modern power grids of the future with high proliferation of renewables and distributed generation, as the system short circuit level increases [19]. Since other protection algorithms such as fault detection and identification in transmission lines heavily depend on the current measurements [20,21], failure in fast detection and reconstruction of distorted currents due to CT saturation negatively affect the performance of protection algorithms and consequently jeopardize the power grid reliability and security.

In the second category, the algorithms mostly focus on the identification of inrush currents to distinguish them from fault signals. In this category, CT saturation is typically considered as a hard case study and the effect of CT saturation is reflected on the threshold of decision making. Such algorithms usually utilize multiple indices whose thresholds depend on the system configuration and parameters and as a result, are case-dependent.

The state-of-the-art algorithms in this area can be categorized as follows:

- *Harmonic restrain methods* [22,23]: which are noncomplex algorithms and highly depend on the second and fifth harmonic currents to distinguish inrush current from fault current. However, as discussed in [24], high flux remanence in transformers and also the presence of series capacitors in transmission lines may result in an escalated second harmonic component in fault conditions. It has

* Corresponding author.
E-mail address: payman@gwu.edu (P. Dehghanian).

https://doi.org/10.1016/j.ijepes.2020.105939
Received 18 September 2019; Received in revised form 3 February 2020; Accepted 11 February 2020

been also discussed in [25] that utilizing new materials in the core of power transformers may also change the harmonic content of the inrush current, thereby adding additional complexity to distinguish between an internal fault and inrush current.

- *Model-based methods* [26–29]: are basically centered on transformer parameters, voltage and flux restrains and also inductance assessments.
- *Artificial intelligence methods* [30–34]: which are based on pattern recognition principles and are implemented with neural networks [30–32] and fuzzy logic [33,34]. As they require large volumes of data for training as well as a large processing memory, such techniques generally suffer from computational complexities.
- *Wavelet transform methods* [35–37]: utilizing wavelet transform results in a more comprehensive view simultaneously in time and frequency domains. However, they need long data windows and are susceptible to noise as well as unanticipated disturbances.
- *Hybrid methods* [25,28–40]: Lately, some innovative methods based on current–voltage signals [25], kurtosis [38], waveform sinusoidal similarity identification [39] and discrete Fréchet distance algorithm [40] have been proposed to distinguish between inrush current and internal faults. However, sensitivity to decaying DC component, dependence on both current and voltage information, and long delay in hard cases are the main drawbacks of such methods.

In almost all the above methods, CT saturation remains a challenging issue, while CT transient response in the CT saturation detection process has been neglected and its effects on the decisions for distinguishing the inrush and fault current signals have not been investigated.

This paper presents an algorithm that enhances immunity of the differential relays during potential mal-operation circumstances (i.e., to distinguish inrush current from fault current even under CT saturation conditions). The proposed scheme is designed based on a high-order statistic moment, the so-called kurtosis, which is applied to the current signals. The proposed scheme offers the following contributions:

- The proposed scheme is designed based on the twofold indices that are assessed based on the kurtosis of the unsaturated sinusoidal components. As it can be mathematically proven, the proposed indices are dependent on the fundamental phase angle. As a result, due to changes in the phase angle, the indices notably and swiftly change under inrush and fault current conditions when the CT is saturated. Note that the proposed method operates based on the twofold indices which consequently requires two thresholds; however, the thresholds are independent of the transformer parameters.
- One major goal of the proposed scheme is to provide fast decision making criteria. The proposed indices are introduced so that they can utilize the first quarter of a cycle. As mentioned, the proposed method only depends on the fundamental phase angle, and not on the magnitude, of the current signal. As a result, the key feature in the proposed algorithm is fast estimation of the fundamental phase angle of the current signal, thereby resulting in an expedited classification of the disturbances. In order to achieve a fast estimation of the phase angle of the current signal, the phasor estimation algorithm in [3] has been employed in which the phasor estimation is conducted in sub-cycle and utilizing unsaturated interval of the current signals.
- Comparisons with the state-of-the-art on CT saturation detection reveals that the suggested method in [3], utilizing multiple indices, almost comprehensively deals with the saturation detection and fault classification using three phase current signals. However, the proposed indices in this paper solely detects the change, classifies the nature of the disturbance, and determines the initial distortion point caused by the saturation in the fault scenarios using single phase current signal.
- Comparison with state-of-the-art on discrimination between inrush and fault current reveals that in [38], a kurtosis based index is suggested for discrimination between inrush and fault current. However, the proposed approach in this paper is different with [38] in that (i) the effects of decaying DC component in the fault current is adequately captured in our technique (i.e. the calculation of fundamental phase angle is conducted based on the algorithm [3] that removes the effect of fault current DC components), and (ii) the proposed technique works based on a sliding window which requires quarter of a cycle data for its estimations, while the method suggested in [38] needs a full cycle data for its assessments, and (iii) unlike [38], which reflects the CT saturation into threshold using multiple simulation scenarios, the proposed method provides a sub-cycle index for detection of the CT saturation.

This paper is organized as follows. Section 2 describes the proposed algorithm and its mathematical formulations. Section 3 presents the implementation procedure of the proposed algorithm. Various case studies are extensively analyzed in Section 4 and eventually come the conclusions in Section 5.

2. Problem statement and proposed algorithm

2.1. Mathematical expressions of fault current signals

According to [41–43], the general expression of the fault current in the secondary side of the CT is as follows:

$$i(t) = I_1 \sin(2\pi ft + \varphi_1) + I_{dc} e^{-t/\tau_{dc}} + I_{CT} e^{-t/\tau_{CT}} \quad (1)$$

where, I_1, I_{dc} and I_{CT} are magnitudes of the fundamental component, decaying direct current (DC) offset caused by the grid and decaying DC offset caused by the CT, respectively. τ_{dc}andτ_{CT} are time constants of the decaying DC offset caused by the grid and CT, respectively. φ_1 represents the phase angle of the fundamental component and f is the system frequency which is equal to 50 Hz.

The proposed method is based on the kurtosis of the second derivative of the current signal in the first cycle following the fault inception. According to [41], the time constant of the power grid and the CT are much larger than quarter of a cycle, meaning that the decaying DC components can be assumed constant during the first half cycle. As a result, the exponential terms in (1) can be linearized as in below:

$$i(t) \simeq I_1 \sin(2\pi ft + \varphi_1) + I_{dc}(1 - \frac{t}{\tau_{dc}}) + I_{CT}(1 - \frac{t}{\tau_{CT}}) \quad (2)$$

Applying two consecutive derivations on (2), the following expressions for the second derivative $i"(t)$ can be concluded:

$$i''(t) = -I_1(2\pi f)^2 \sin(2\pi ft + \varphi_1) = A \sin(2\pi ft + \varphi_1) \quad (3)$$

where, A is an interim parameter.

2.2. Kurtosis

The kurtosis is the fourth order normalized moment which is used to describe the shape of the probability density function (PDF) [44]. Assuming X as a random variable, the kurtosis is defined as follows:

$$Kurtosis[X] = K = \frac{E[(X - \mu_a)^4]}{(E[(X - \mu_a)^2])^2} \quad (4)$$

It is assumed that the sample time t_i is a random variable in the arbitrary time window T_a of the samples and t_i has a uniform PDF in the arbitrary window T_a. According to (4), the kurtosis of $i"(t)$ is calculated as below:

$$Kurtosis[i''(t)] = K = \frac{E[(i''(t) - \mu_a)^4]}{(E[(i''(t) - \mu_a)^2])^2} \quad (5)$$

where $i"(t)$ represents the second order derivative of the current signal $i(t)$. Also μ_a is the mean value of $i"(t)$ and is defined as follows:

$$\mu_a = E[i''(t)] = \frac{1}{T_a}\int_{t-T_a}^{t} i''(t)dt = \frac{1}{T_a}\int_{t-T_a}^{t} A\sin(2\pi ft + \varphi_1)dt \quad (6)$$

Calculating (6), μ_a is achieved as follows:

$$\mu_a = \frac{\cos\varphi_1 - \cos(T_a\omega + \varphi_1)}{T_a\omega} \quad (7)$$

where T_a represents the length of the window which is selected as an arbitrary parameter. By substituting (7) to (5), the following expression for K is achieved:

$$K = \frac{\frac{1}{T_a}\int_{t-T_a}^{t}(A\sin(2\pi ft + \varphi_1) - \mu_a)^4 dt}{\left(\frac{1}{T_a}\int_{t-T_a}^{t}(A\sin(2\pi ft + \varphi_1) - \mu_a)^2 dt\right)^2} \quad (8)$$

With the integration (8) evaluated, K is generally expressed as follows:

$$K = \frac{\sum_{i=1}^{4} Y_i}{\sigma_a^4} \quad (9)$$

where Y_i and σ_a are the interim variables that are assessed in the following:

$$Y_1 = \frac{3}{8} + \frac{\cos 2\varphi_1 - \cos(2\omega T_a + 2\varphi_1)}{2\omega T_a} + \frac{\cos 4\varphi_1 - \cos(4\omega T_a + 4\varphi_1)}{32\omega T_a} \quad (10)$$

$$Y_2 = 3\mu_a^2\left(1 + \frac{\sin 2\varphi_1 - \sin(2\omega T_a + 2\varphi_1)}{2\omega T_a}\right) \quad (11)$$

$$Y_3 = 3\mu_a\frac{\cos(T_a\omega + \varphi_1) - \cos\varphi_1}{T_a\omega} - \mu_a\frac{\cos(3T_a\omega + 3\varphi_1) - \cos 3\varphi_1}{3T_a\omega} \quad (12)$$

$$Y_4 = -3\mu_a^4 \quad (13)$$

$$\sigma_a = \sqrt{\frac{1}{2} - \frac{\sin 2\varphi_1 - \sin(2T_a\omega + 2\varphi_1)}{4T_a\omega} - \mu_a^2} \quad (14)$$

As can be seen in (9) to (14), there are two important parameters that should be selected. On the parameter selection, Fig. 1 presents sensitivity of K to variations in T_a and φ_1. One can realize, in Fig. 1, that for the window length less than half a cycle, the variations of the kurtosis in both value and polarity are significant, while for the window length greater than half a cycle, the changes in kurtosis values are comparably very small. It reflects the fact that as the window length increases, the sensitivity of the kurtosis to phase angle goes ideally toward zero. However, the algorithm to calculate the signal phase angle may need different window lengths. Here, T_a dictates the delay of the kurtosis or K to reach an authenticated value for decision making. According to Fig. 1, the variations in phase angle is determinant for each T_a, and hence, T_a is here selected equal to quarter of a cycle.

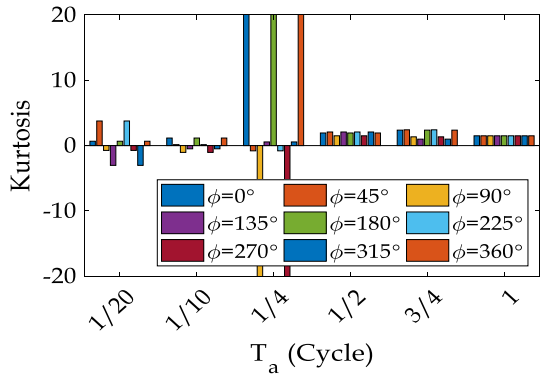

Fig. 1. The sensitivity of kurtosis to variations in T_a and φ_1.

2.3. Disturbance classification and saturation detection

All calculations given in the previous subsection are based on the fact that the fault signal preserves the general format as represented in (1). However, it is found that the inrush or saturation phenomena will create distortions in the current signal that may potentially result in a current signal that may not necessarily fit in expression (1).

In order to distinguish an unsaturated fault condition, inrush current, and saturated fault conditions, the following criteria are presented for relay decision making:

Criterion 1: For making distinctions between inrush current and fault conditions, an index called disturbance classification index (*DCI*), is defined as in (15):

$$DCI = 1 - std(K) \quad (15)$$

where, *std* is the standard deviation. According to (15), if the *DCI* is smaller than a threshold, then the signal is inrush current, while it is a fault signal otherwise. To justify the selection of this criterion, it should be noted that the expression (15) depends on the variations in K, where the inrush current can be simply identified following a disturbance. This is due to the fact that K in (9) only depends on φ_1 which is a time-variant parameter for inrush current and an almost constant value for fault currents. As a result, the variations in φ_1 and consequently K will result in a significant change in the *DCI* when an inrush current appears.

In order to detect CT saturation under the fault conditions, if *DCI* is smaller than a threshold, then the saturation is detected. In other words, if the *DCI* remains constant and close to 1, it reflects that the CT is not saturated. This is because the phase angle is a constant value in the unsaturated portion of the signal, and as a result, the values of K and the *DCI* are almost constant in the unsaturated portion of the signal. However, the estimated phase angle in the unsaturated portion of the signal becomes highly distorted due to the fact that the saturated signal no longer fits in (3). Hence, the *DCI* value violates the threshold.

Note that the difference between the cases of inrush and saturated current signals is that in the former, the signal is highly distorted from the beginning (i.e. exactly after happening), while in the latter (even if a deep CT saturation occurs), the fault current remains unsaturated at about 1/6 of the cycle.

Criterion 2: The kurtosis index (*KI*) for relay decision making to distinguish between inrush and fault current signals even in the presence of CT saturation is proposed as follows:

$$KI = \left|1 - \frac{1}{1 + K_R}\right|$$
$$K_R = std\left(\left|\frac{K_{SD}}{K_\varphi}\right|\right) \quad (16)$$

where, K_{SD} and K_φ are kurtosis values based on the second order derivative of the current signal and estimated phase angle, respectively. Also, K_R is the ratio of the K_{SD} and K_φ. If a fault happens, the estimated value of K_{SD} which is calculated in each a quarter of a cycle, and K_φ which is calculated every 1 ms following the disturbance, are almost the same. As a result, the value of *KI* remains close to zero (less than a threshold). Note that to cover probable CT saturation in the first quarter of the cycle, the proposed method delays the decision making for a quarter of a cycle after the disturbance occurrence. If DCI identifies a CT saturation scenario in less than a quarter of a cycle after disturbance, then the KI uses unsaturated interval phase angle for estimating K_φ. Otherwise, KI uses the phase angle estimated from the quarter of a cycle. In both the un-saturated and saturated fault conditions, variance of K_R remains low since both K_{SD} and K_φ are almost in the same range. As a result, KI ideally reaches below threshold after about a quarter of a cycle. However, in the inrush currents, the values of K_{SD} and consequently K_R change notably so that the KI index crosses the threshold.

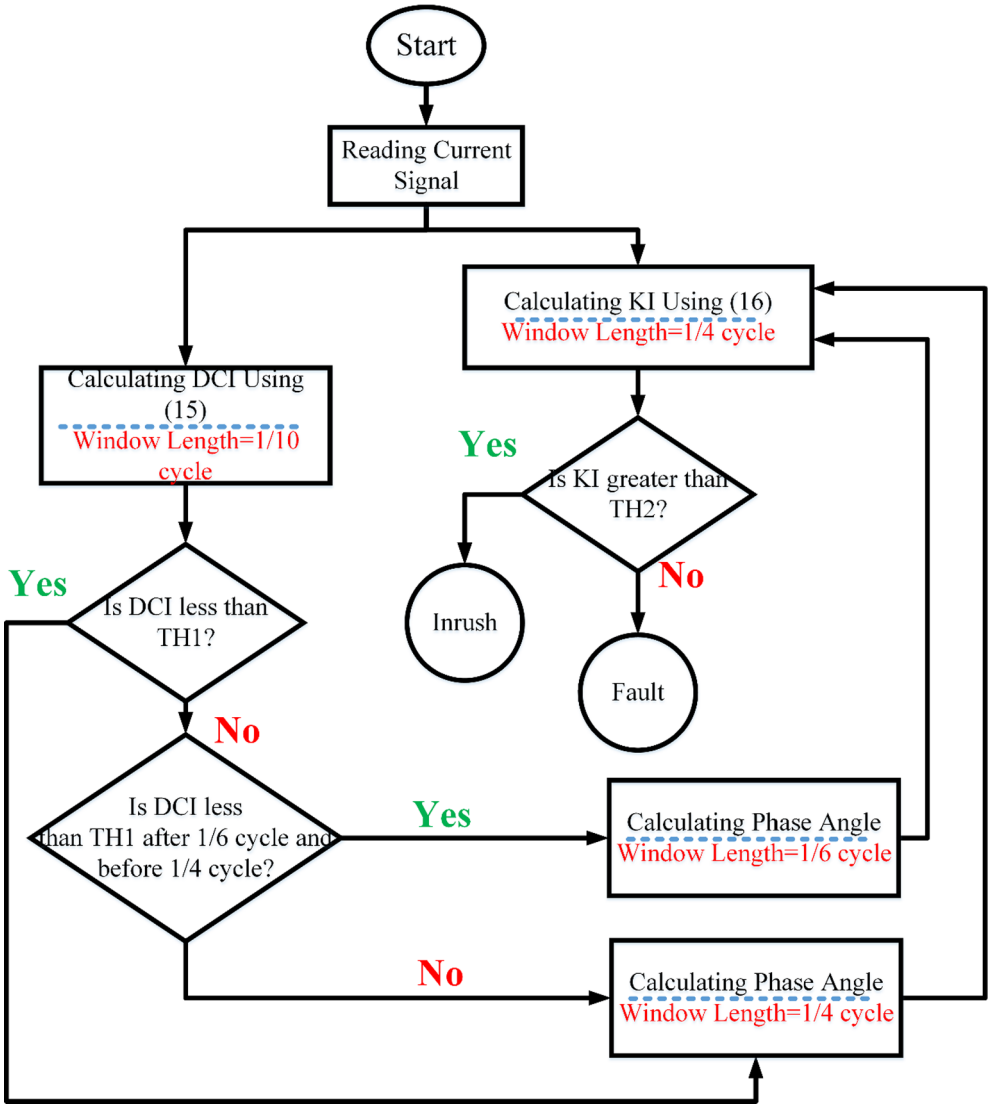

Fig. 2. The implementation procedure of the proposed scheme.

3. Implementation

To implement the proposed scheme, expression (9) calls for assessment of the phase angle. As discussed earlier, it is essential to estimate the phase angle in less than 1/6 cycle following the disturbance particularly under deep CT saturation scenarios. Here, the sub-cycle phasor and parameter estimation algorithm in [3] is employed, in which we assume a 240 sample/cycle sampling rate with which only 12 samples (or about 1/20 of a cycle) are required to estimate the fundamental phase angle. The procedure of calculating the phase angle is provided in Appendix 1. Note that the potentials in using high-sampling rate for protection applications in digital relays have been fully discussed in [45,46].

The implementation procedure of the proposed scheme is illustrated in Fig. 2. Basically, the calculations of DCI and KI start in parallel. However, KI requires the decision of DCI for two conditions: first to preliminary distinguish between the inrush and fault conditions, and second, to check whether saturation is detected in the first quarter of a cycle. To be more specific, the procedure is based on the following steps:

Step 1: With the current signal acquired, the fundamental phase angle is calculated and consequently fed into (15) and (16) to estimate the *DCI* and *KI*, respectively.

Step 2: Overall, the *DCI* has two goals: first discrimination between the fault and inrush signal exactly after disturbance occurrence, and second, finding the saturation in the first quarter of a cycle. Comparison of the estimated *DCI* and a threshold value (TH1), the decision to distinguish the fault from inrush current and also on CT saturation detection is made as follows:

- *DCI* distinguishes between inrush current and fault conditions exactly following the disturbance inception. It means after about 2 ms, if the *DCI* remains above the threshold, the disturbance is identified as fault.
- The saturation detection based on the *DCI* is performed following the observation on *DCI* crossing the threshold after at least 1/6 cycle (i.e. deep saturation condition). Note that the saturation may not happen in the first quarter of the cycle and, as a result, the phase angle will not be affected in this interval due to the distortions caused by CT saturation.

Step 3: If *DCI* detects a CT saturation incident, then *KI* assessment should be performed based on the unsaturated interval. Otherwise, the *KI* requires a quarter of a cycle signal for decision making. Based on the window length for the required data, a quarter of a cycle from the current signal is ideally required for an accurate decision making.

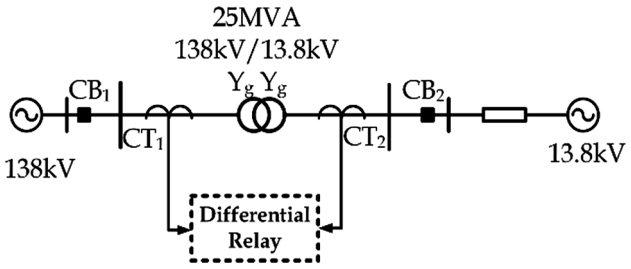

Fig. 3. The simulated test system.

It should be noted that assuming 240 samples per cycle, the phase angle is evaluated with 12 samples (about 1 ms). However, the *DCI* is based on the variance in *K* and is calculated based on the subsequent 1 ms (i.e., 12 consecutive samples of *K*). As a result, decision making based on the *DCI* requires about 24 samples (about 2 ms). Discussions on selection of TH1 and TH2 considering noisy and harmonic conditions are provided in the next Section.

4. Simulation results and discussions

The performance of the proposed method is evaluated on a simulated test system presented in Fig. 3, where the system characteristics are adopted from [25]. Low voltage and high voltage sides of the power transformer are provided by two CTs with specifications of 1200/5 and 100/5, respectively. Also, the magnetization characteristics taken into account for simulation of the CTs are taken from. The specifications of the test system are provided in Appendix 2. The test system and the proposed methodology are implemented in MATLAB programming environment. Also, the performance of the proposed method is compared with the second harmonic restrain (SHR) method. Studies on more than 1765 scenarios including 625 inrush current signals and 1140 internal and external fault current signals with/without CT saturation are conducted considering different fault type scenarios (single-phase, double-phase, three phase to ground), fault inception angles (0 to 360°), fault resistance (0 to 5 Ohms), transformer energization instance (0 to 360°), remanence level of power transformer (-80% to + 80%), and noise level (40 dB to 60 dB). Here, we present some of the simulations and experimental tests to demonstrate the performance of the proposed algorithm. Investigating the performance of the *DCI* by applying 1765 scenarios, it has been observed that *DCI* is not exceeded 0.94. This is because the variation of phase angle and consequently *K* by (9) is very low in the case of fault without saturation. As a result, the threshold, *DCI TH*1, is selected 0.9 for a safe decision making. Similarly, the threshold for the proposed technique (*TH*2) is obtained from applying 1765 scenarios. It should be noted that the proper value of *TH*2 varies between 0.05 and 0.15 in different test scenarios. This is because phase angle estimation algorithm uses sub-cycle data and despite all considerations, the transients in fault current signal may affect the approximated phase angle, and consequently, *K* by (9). One important observation is that the lower threshold guarantees the reliability of the relay's decision making at the cost of additional delays [22]. To validate the timing performance of the proposed method under the worst case scenarios, the threshold for *TH*2 is selected 0.05. Note that the threshold on the SHR (SHR_T) is selected 0.15. In all cases, the magnitudes of the current signals of phase A are provided in per unit. Also, DIT, DDT, and FPoC respectively stand for the disturbance inception time, disturbance detection time, and first point of convergence to authenticated value. The change detection presented in [3] was applied on the signals to identify the abnormal conditions against the load change scenarios. In other words, the applied signal into the proposed method is somehow filtered to categorize between fault, fault with saturation and inrush current signals. According to [3], if a change happens and the magnitude of the current signal in all phases vary higher than a certain threshold in the pre-disturbance

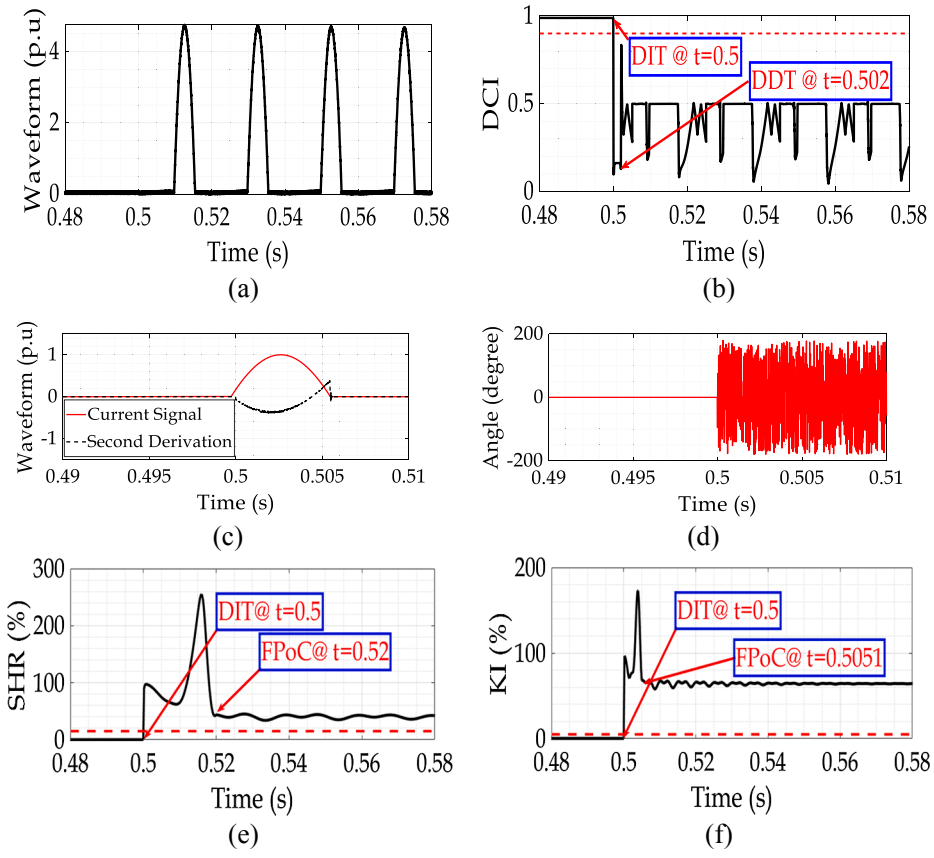

Fig. 4. Evaluating the performance of the proposed algorithm for inrush current (remnant flux of the power transformer is assumed zero): (a) current signal, (b) disturbance classification index, (c) scaled current signal and its derivation, (d) estimated phase angle through the derivation of the current signal, (e) second harmonic restrain method, (f) proposed method.

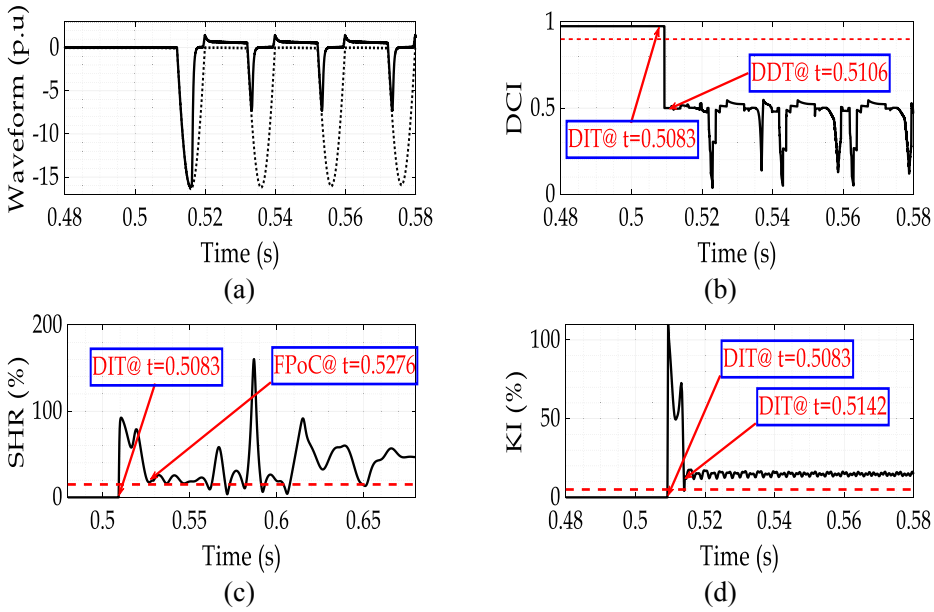

Fig. 5. Evaluating the performance of the proposed algorithm for inrush current (remnant flux of the power transformer is assumed 80% of the knee point flux): (a) current signal, (b) disturbance classification index, (c) second harmonic restrain method, (d) proposed method.

condition, the signal is assumed to be originated from an abnormal condition. In this paper, the threshold was assumed 50% of the magnitude of the current signal.

4.1. Inrush current

Figs. 4 and 5 illustrate the performance of the proposed algorithm on two inrush current signals in which the remnant flux of the power transformer is 0 and 80%, respectively. As can be seen in these figures, the proposed *DCI* reaches below the threshold (red dashed line) just after about 2 ms following the disturbance inception. As it can be seen in Fig. 4.c and d, considering (3) as the reference function for phase angle estimation, the approximated phase angle has significant variations since the shape of the inrush current is no longer similar to the sinusoidal function. It should be noted that in Fig. 4.c, the current signal and its derivation are scaled for better illustrations.

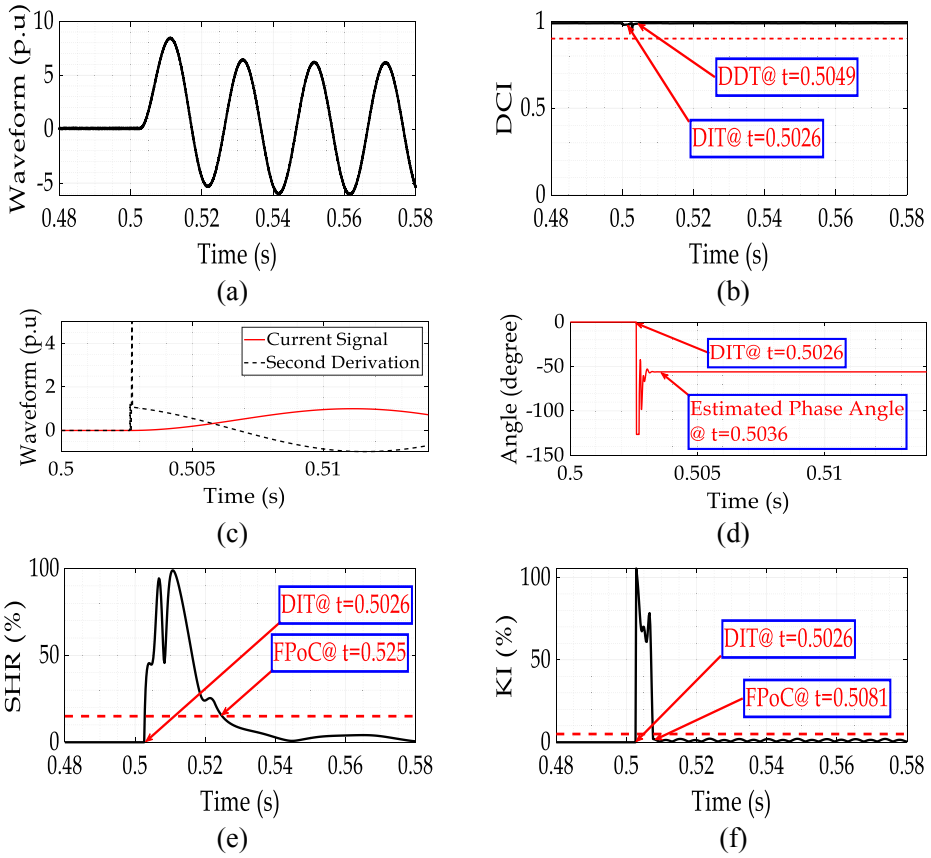

Fig. 6. Evaluating the performance of the proposed algorithm for fault current without CT saturation: (a) current signal, (b) disturbance classification index, (c) scaled current signal and its derivation, (d) estimated phase angle through the derivation of the current signal, (e) second harmonic restrain method, (f) proposed method.

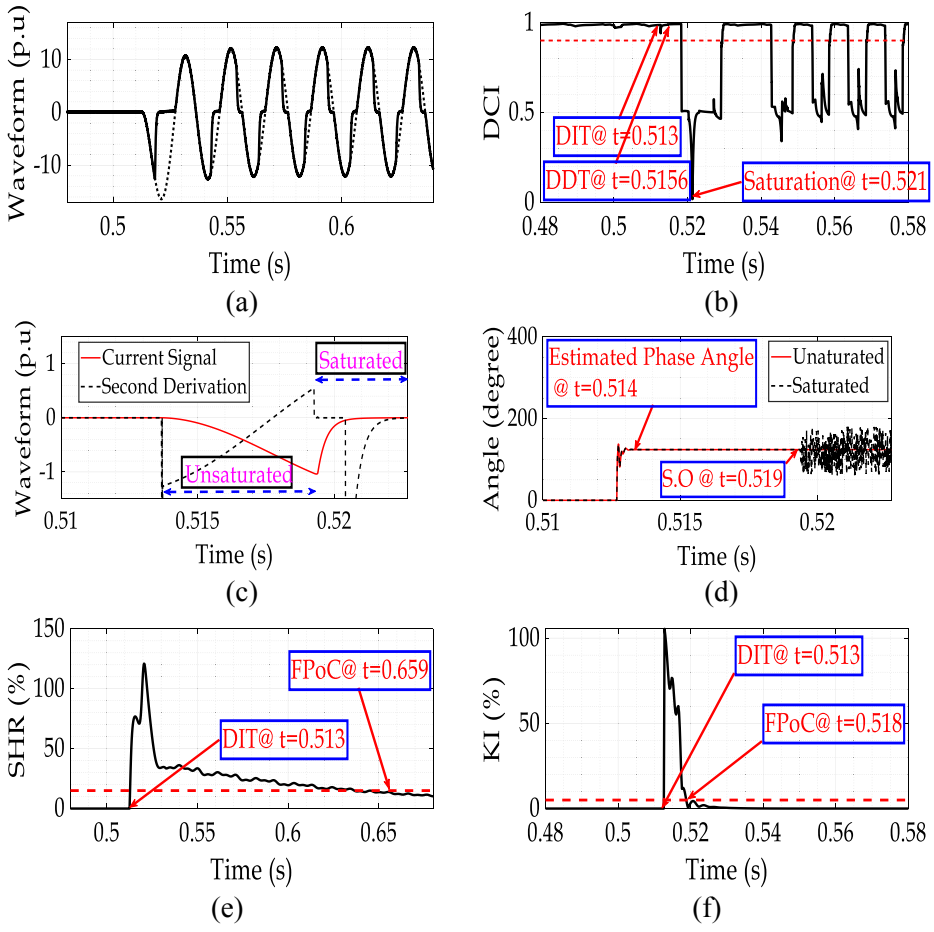

Fig. 7. Evaluating the performance of the proposed algorithm for fault current with CT saturation: (a) current signal, (b) disturbance classification index, (c) scaled current signal and its derivation, (d) estimated phase angle through the derivation of the current signal, (e) second harmonic restrain method, (f) proposed method.

As seen in Fig. 4, both SHR and the proposed method offer appropriate marginal distances to the threshold and both methods have not operated in response to the inrush current (i.e., ensured dependability). The difference between the SHR and *KI* is that the proposed method has reached the authenticated value after about 5 ms while the SHR method achieves it after about 20 ms.

Also, as it can be seen in Fig. 5, in the case of CT saturation due to remnant flux in the power transformer, the SHR shows unreliable operation after one cycle. As can be seen in Fig. 5.c, the DIT reaches the authenticated value in one cycle following the disturbance, but in an unstable manner that results in unreliable decision making. In comparison with SHR, *KI* reveals more appropriate marginal distance to the threshold after about 6 ms.

4.2. Fault current with/without CT saturation

Figs. 6 and 7 show the performance of the proposed method on two fault current signals. As can be seen, the *DCI* remains on top of the threshold (red dashed line) for unsaturated fault current in Fig. 6. b. *DCI* remains on top of the threshold since according to Fig. 6.c and d, the estimated phase angle remains constant due to similarity in the shape of the derivation to a sinusoidal function. Additionally, according to Fig. 7.b, for the saturated fault current scenario, the *DCI* remains well beyond the threshold in unsaturated interval and goes under threshold just about 2 ms after the instant when the current signal becomes distorted. The estimated phase angle in Fig. 7.d demonstrates why *DCI* crosses the threshold after saturation occurrence (S.O). It should be noted that saturation time given in Fig. 7.b is the saturation time that the proposed *DCI* is determined and it is 2 ms after S.O.

As can be seen in Figs. 6 and 7, both SHR and the proposed method offer appropriate marginal distances to the threshold and both methods have successfully operated on fault currents (i.e., ensured security). However, the difference between the SHR and *KI* is that the proposed method has reached the authenticated value after about 5 ms while the delay corresponding to the SHR is about 20 ms.

4.3. Internal fault with inrush currents

Effectiveness of the proposed method for transformer energization with an internal fault incident is shown in Fig. 8. As can be seen, the *DCI* remains on top of the threshold (red dashed line). Note that during transformer energization with internal fault, the voltage across the magnetization branch of the power transformer in the faulty coil is not allowed to increase similar to unfaulty coils. As a result, the current waveform in the faulty coil is more similar to the fault current than the inrush current. Therefore, the *DCI* value remains well above the threshold. As can be seen in Fig. 8, the SHR method provides an unstable output and it takes about 3.5 cycles for the relay to identify the signal as the fault current. In other words, the SHR in such circumstances fails with no expected operation for 3.5 cycles (i.e., compromised security). However, the proposed method has reached the authenticated value in about 12 ms (i.e., ensured security).

4.4. Performance evaluation through experimental data

In order to further evaluate the performance of the proposed method with experimental data, a set-up including a single-phase transformer bank with the specifications of 2 kVA, 220 V:100 V, 50 Hz

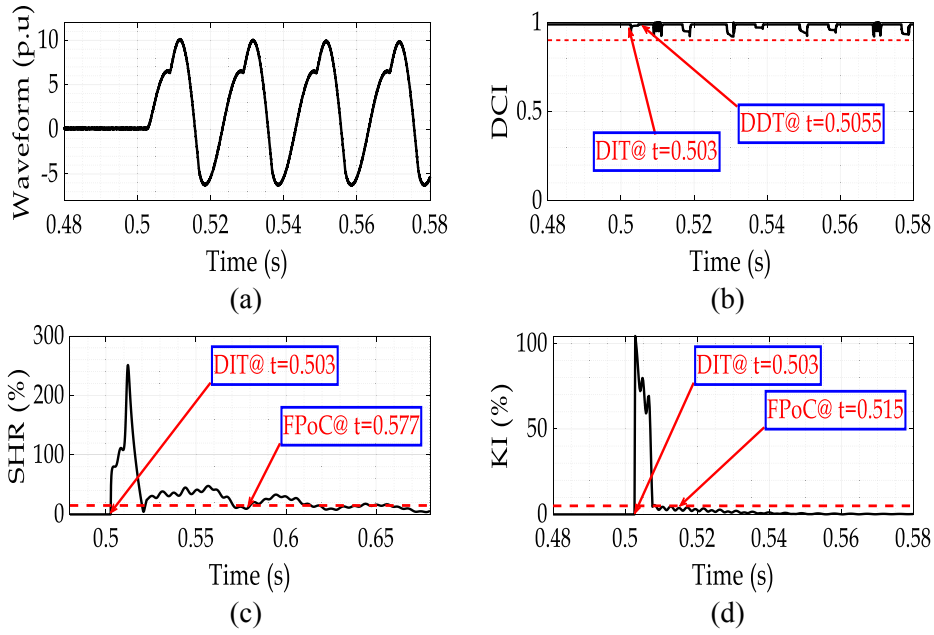

Fig. 8. Evaluating the performance of the proposed algorithm for internal fault current without CT saturation (20% of the secondary winding of the power transformer in phase A is solidly grounded): (a) current signal, (b) disturbance classification index, (c) second harmonic restrain method, (d) proposed method.

was provided as shown in Fig. 9. Several inrush and internal fault scenarios were applied and recorded with a sampling rate of 4.8 kHz and then resampled with sampling rate of 12 kHz to apply in the proposed algorithm and SHR method. We here describe two scenarios.

Fig. 10 shows the performance of the proposed method in an experimental inrush current scenario. As can be seen, both the proposed method and the SHR method have successfully identified the current signal as an inrush current (i.e., ensured dependability). The main difference between the SHR and the proposed method is that the latter converges to a reliable output (*KI*) after about 5 ms as shown in Fig. 10.d, while the former converges to the authenticated value after 23 ms. In cases of internal faults during transformer energization, it can be seen in Fig. 11.c that the SHR has failed to detect the fault condition for almost 9 cycles (i.e., compromised security) while the proposed method converges to the authenticated value after only 5 ms with a reliable distance to the threshold (i.e., ensured security).

Analyzing different simulated and experimental scenarios with extensive performance evaluations revealed that in comparison with the SHR method, the proposed approach can quickly and also precisely tackle various challenging concerns on differential protection such as inrush with/without CT saturation, internal fault with/without CT saturation, and eventually internal fault with transformer energization. Moreover, the proposed approach can mathematically guarantee a promising immunity against unwanted effects of decaying DC components in power systems and due to CT transient response.

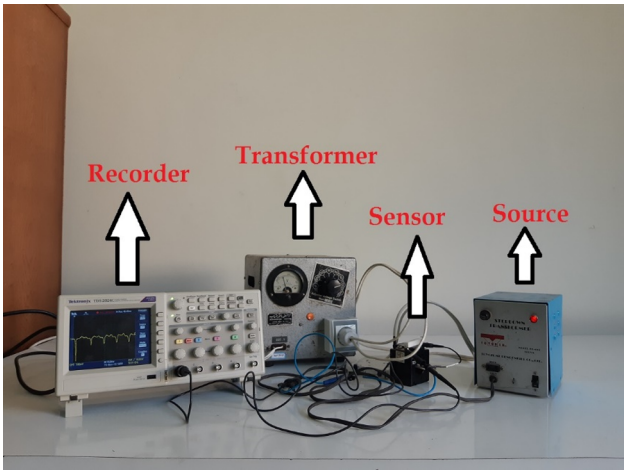

Fig. 9. Experimental set-up including a single-phase transformer for evaluating the performance of the proposed algorithm.

4.5. Performance of the proposed index for Y/Δ connection of power transformer

This section discusses the performance of the proposed index for Y/Δ connection of power transformers. To this end, the Y/Y connected power transformer in the single-line diagram presented in Fig. 3 was replaced with a Y/Δ connected power transformer. Several fault and inrush scenarios were applied to the test system. In the following, three scenarios are selected to evaluate and discuss the performance of the proposed method.

In the *first scenario*, Fig. 12 shows the performance of the proposed algorithm on an inrush current signal in which the remnant flux of the power transformer is 30%. As can be seen in this figure, the proposed *DCI* reaches below the threshold (red dashed line) just after about 2 ms following the disturbance inception. Also, according to Fig. 12, in the case where the remnant flux is present in the power transformer, the SHR shows unreliable operation after one cycle. As can be seen in Fig. 12.c, the DIT reaches the authenticated value in one cycle following the disturbance, but in an unstable manner that results in unreliable decision making. In comparison with SHR, *KI* reveals more appropriate marginal distance to the threshold after about 5 ms.

In the *second scenario*, Fig. 13 shows the performance of the proposed method on a fault current signal with CT saturation. As can be seen in this figure, for the saturated fault current scenario, the *DCI* remains well beyond the threshold in unsaturated interval and goes below the threshold just about 2 ms after the instant when the current signal becomes distorted. As can be seen in Fig. 13, the proposed method offers appropriate marginal distances to the threshold and the proposed method has successfully operated on fault currents. Also, a difference between the SHR and *KI* is that the proposed method has reached the authenticated value after about 5 ms while the delay attributed to the SHR is about 60 ms.

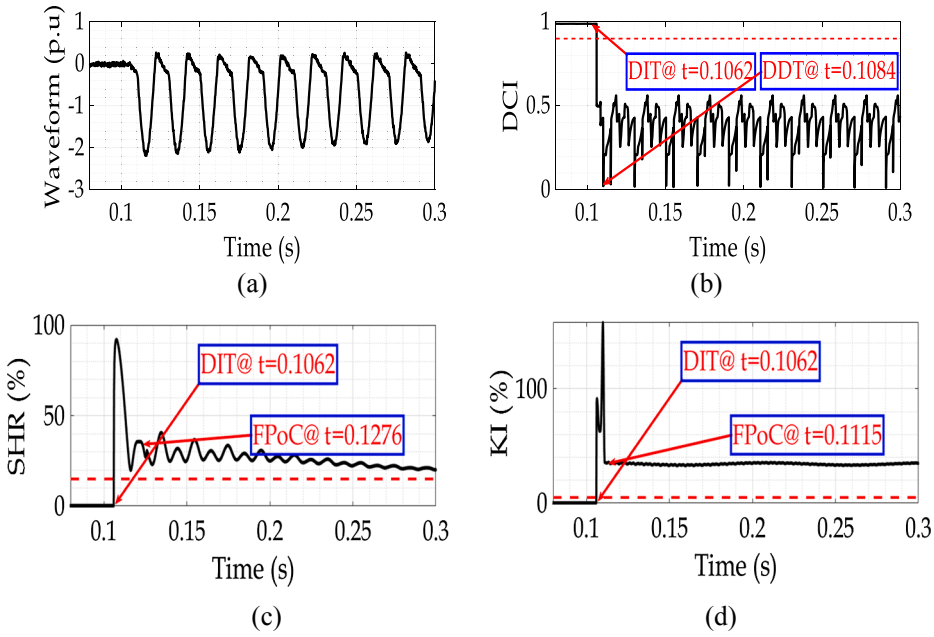

Fig. 10. Evaluating the performance of the proposed algorithm for experimental recorded inrush current: (a) current signal, (b) disturbance classification index, (c) second harmonic restrain method, (d) proposed method.

Eventually, in the *third scenario*, the performance of the proposed method for transformer energization with an internal fault incident is shown in Fig. 14. As can be seen in this figure, the *DCI* remains beyond the threshold (red dashed line). As previously mentioned, during transformer energization with internal fault, the voltage across the magnetization branch of the power transformer in the faulty coil does not increase similar to unfaulty coils. Therefore, the current waveform in the faulty coil is similar more to the fault current than the inrush current. As a result, the *DCI* value remains well above the threshold. According to Fig. 14.c, the SHR method shows an unstable output, taking about 3 cycles for the relay to identify the signal as the fault current. In other words, the SHR in such circumstances fails with no expected operation for 3 cycles. On the contrary, the proposed method has reached the authenticated value in about 6 ms.

4.6. Performance of the proposed index in the case of sympathetic inrush

This section is provided to evaluate the performance of the proposed method during sympathetic inrush phenomenon. To this end, a power transformer was installed in parallel with the power transformer according to single line diagram presented in Fig. 3. Both transformers are of Y/Δ connections, the specifications of which are given in Appendix 2. In the following case study, T#1 is assumed in-service power transformer, while T#2 is the energizing transformer.

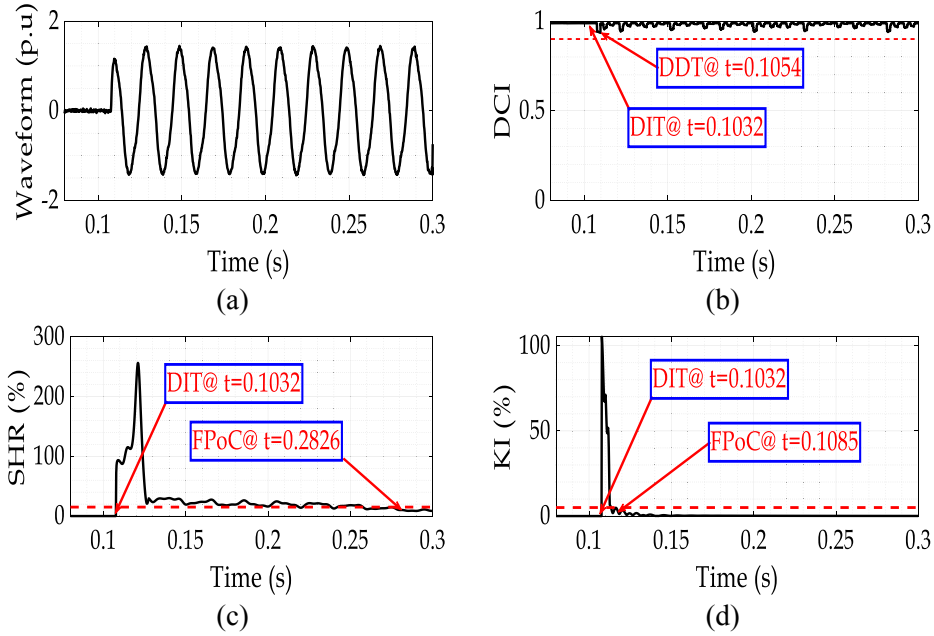

Fig. 11. Evaluating the performance of the proposed algorithm for experimental recorded internal fault current during transformer energization (5% turn to turn of the secondary winding): (a) current signal, (b) disturbance classification index, (c) second harmonic restrain method, (d) proposed method.

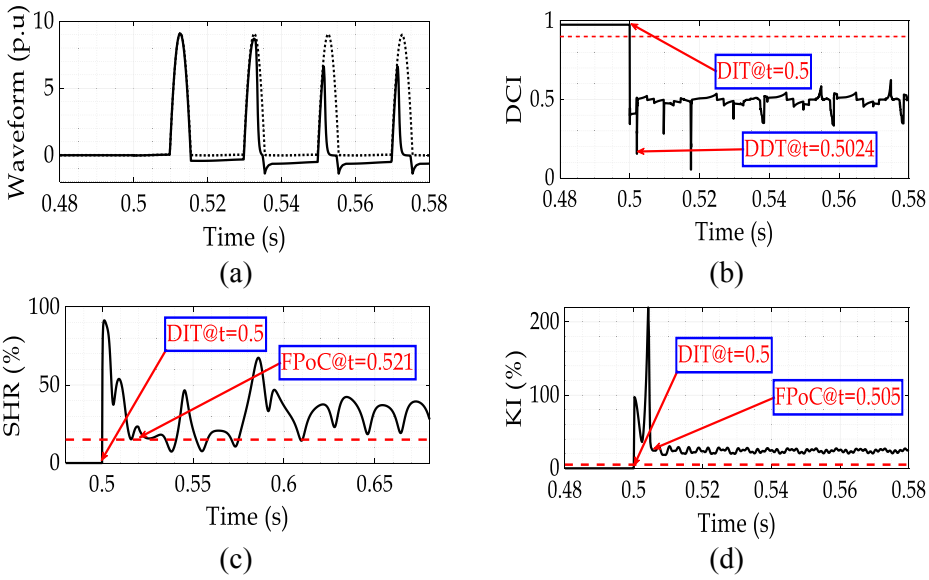

Fig. 12. Evaluating the performance of the proposed algorithm for inrush current (remnant flux of the power transformer is assumed 30% of the knee point flux): (a) current signal, (b) disturbance classification index, (c) second harmonic restrain method, (d) proposed method.

The inrush current signals of the transformers are illustrated in Fig. 15. a. As it can be seen in Fig. 15.b, the *DCI* can effectively recognize the inrush current in both transformers after 2 ms. Note that the distortions in the inrush current signal is magnified via second order derivation. As a result, the difference between inrush and sinusoidal function lead to variations in the estimated phase angle and as a result *K*. It should be mentioned that unlike previous case studies, the value of *DCI* during the sympathetic inrush scenario is near, but lower than, the thresholds. While both *KI* and *SHR* indices have correctly identified inrush current in 5 and 20 ms respectively for T#2, they introduce several challenges in the case of sympathetic inrush. *SHR* has a delay of 3 cycles from the disturbance occurrence. As it can be seen in Fig. 16.b, the second harmonic level during the sympathetic inrush is very low in the first cycles and simulation results in Fig. 16.b indicate that the *SHR* method reveals a poor performance. While the performance of *KI* in the case of sympathetic inrush is not as good as that for the inrush cases given in Section 4.1, the *KI* still can reach to an authenticated and correct identification 19 ms after the disturbance occurrence.

4.7. Discussions on the performance of the proposed index

This section is dedicated to discussions regarding the performance of the proposed index from the technical and computational burden perspectives.

Focusing on the simulated inrush current signals, the delays in SHR and the proposed method for all 625 inrush current scenarios are assessed. As can be seen in Fig. 17, the delay for SHR ranges between about 1 cycle and 5.5 cycles. Long delays belong to the hard cases such as inrush current with CT saturation in which the second harmonic component may become smaller so that the samples of the SHR index are not able to remain on top of the threshold for multiple consecutive time intervals. As discussed in [22], one approach to overcome the

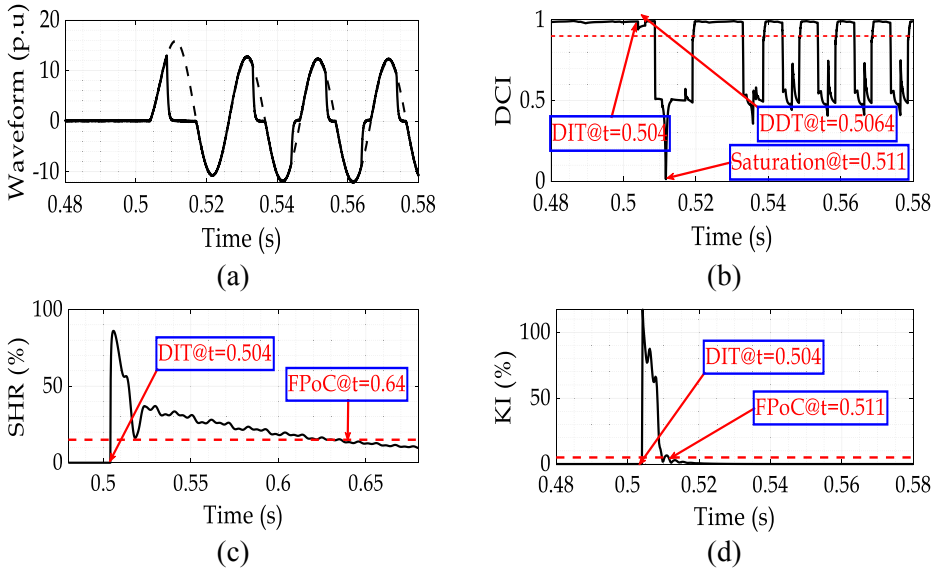

Fig. 13. Evaluating the performance of the proposed algorithm for fault current with CT saturation: (a) current signal, (b) disturbance classification index, (c) second harmonic restrain method, (d) proposed method.

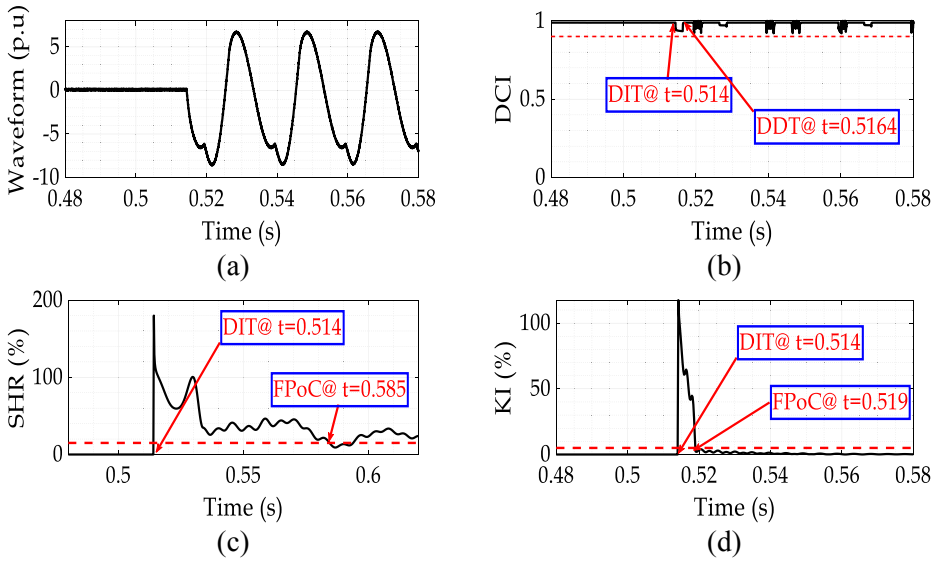

Fig. 14. Evaluating the performance of the proposed algorithm for internal fault current without CT saturation (25% of the secondary winding of the power transformer in phase A is solidly grounded): (a) current signal, (b) disturbance classification index, (c) second harmonic restrain method, (d) proposed method.

latter issue is to re-adjust (lower) the SHT threshold which, in turn, enhances the decision reliability, but at the cost of additional delays. Comparing with the SHR method, the proposed approach reveals a very fast response time with a delay between 4.4 and 16.2 ms. This is achieved primarily due to the fact that the proposed method is centered on the variations in a kurtosis based index, which results in a swift and precise decision making.

Similar to the inrush current scenarios, the delays in SHR and the proposed method are estimated in all 1140 fault scenarios. It can be seen in Fig. 17 that the SHR method reveals a delay between 24 and 124 ms. CT saturation results in distortion introduced in the fault current signals in a way that the second harmonic component may increase, and as a result, samples of the SHR index are not able to reach below the threshold for multiple consecutive time intervals. Compared to the SHR method, the proposed method shows a very quick response time with a delay between 4.6 and 17 ms.

The performance of the proposed algorithm is evaluated under high impedance fault (HIF) incidents near the transformer terminals. For fault resistance between (10, 100) Ohms, 460 fault scenarios have been generated and applied to the investigated methods. As one can see in Fig. 17, the delay of the SHR method is observed varying between 67 and 154 ms with the mean value of about 98 ms. Comparing with SHR method, KI has a very quick response time and the time delay does not exceed about one cycle at the worst case scenario.

Fig. 18 provides a comparison between the computational time of the SHR and *KI* methods for 625 inrush scenarios, 1140 fault scenarios, and 460 HIF scenarios. Note that the computational time is determined following a fault initiation until the method reaches a correct decision. Also, note that the methods have been implemented utilizing a Pentium-4, 2.66 GHz processor with 2 GB RAM. As it can be seen in Fig. 18, the computational time of the KI in the case of inrush scenarios is higher, in the case of fault scenarios is lower, and in the case of HIF

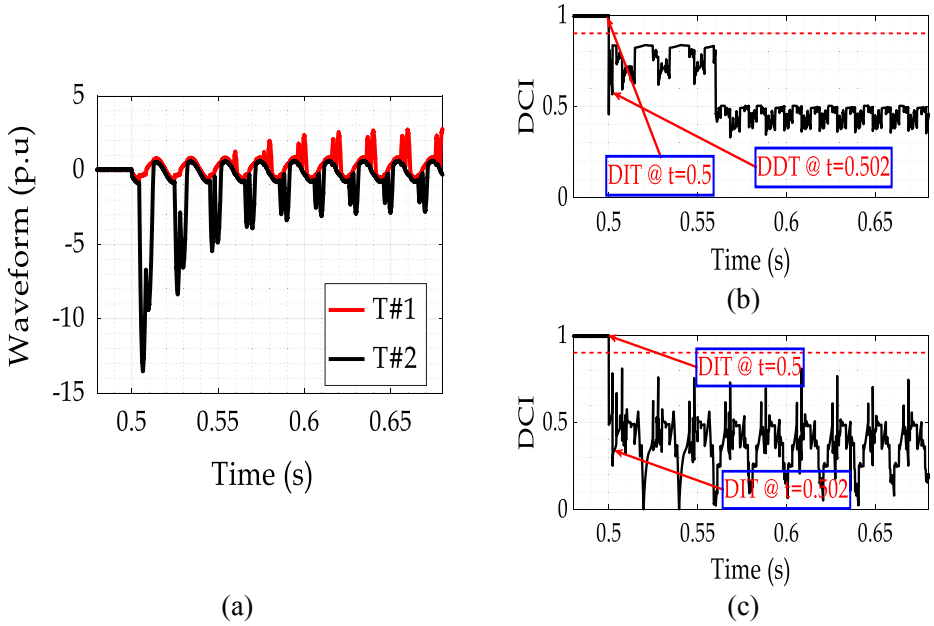

Fig. 15. Performance evaluation of the proposed algorithm for inrush and sympathetic inrush scenarios in two test systems given in Fig. 3, (a) current signal, (b) disturbance classification index (T#1), (c) disturbance classification index (T#2).

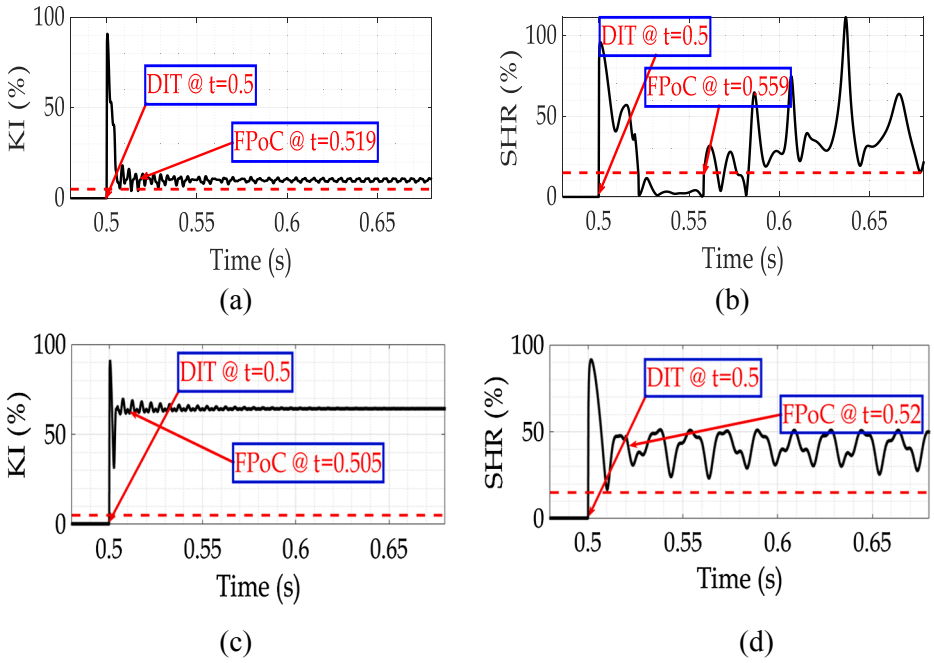

Fig. 16. Performance evaluation of the proposed algorithm for inrush and sympathetic inrush in two test systems given in Fig. 3, (a) second harmonic restrain method (T#1), (b) proposed method (T#1), (c) second harmonic restrain method (T#2), (d) proposed method (T#2).

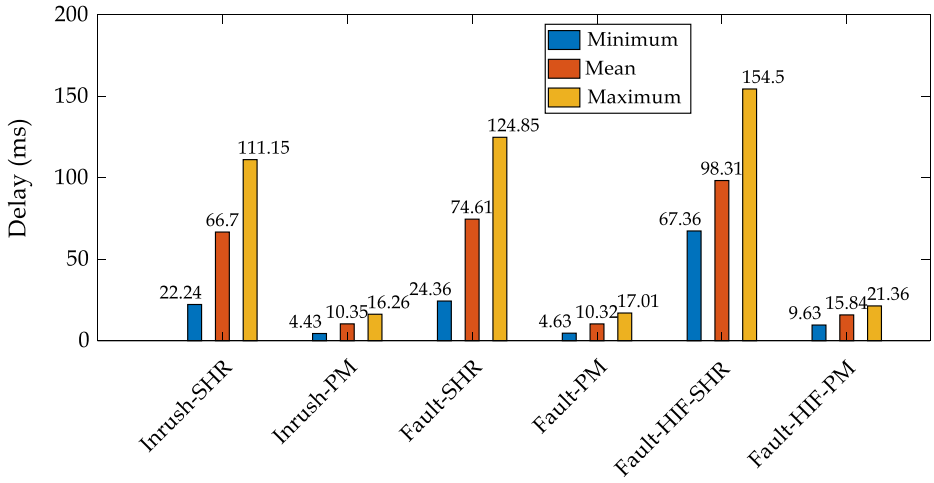

Fig. 17. Comparison between response delay of the SHR and *KI* methods for 625 inrush scenarios, 1140 fault scenarios, and 460 high impedance fault scenarios.

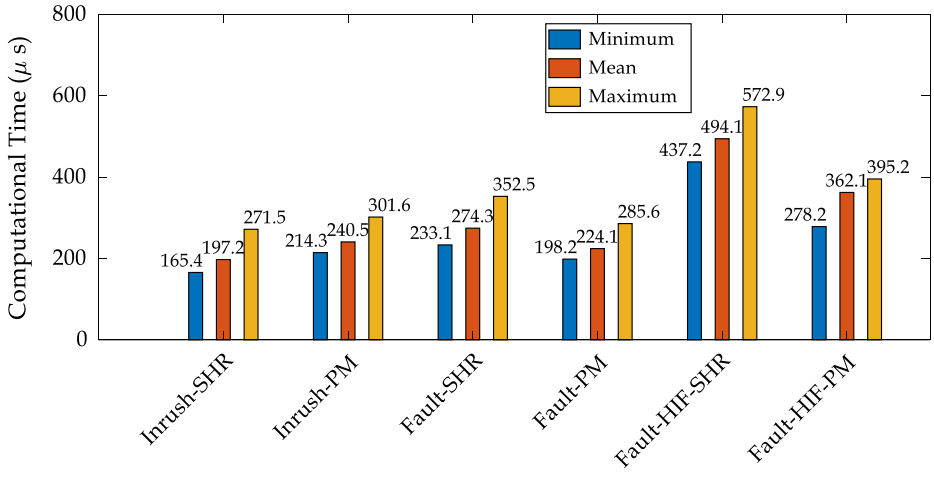

Fig. 18. Comparison between computational time of the SHR and *KI* methods for 625 inrush scenarios, 1140 fault scenarios, and 460 high impedance fault scenarios.

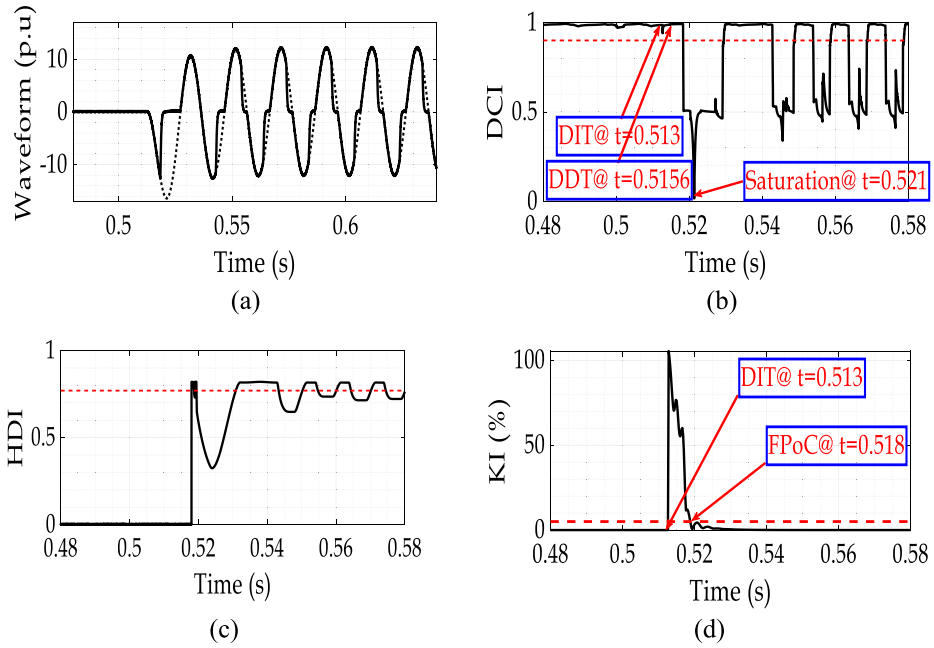

Fig. 19. Evaluating the performance of the proposed algorithm on fault current with CT saturation for Y/Y-connected transformers: (a) current signal, (b) disturbance classification index, (c) Hausdorff distance based algorithm, (d) proposed method.

scenarios is notably lower than that for the SHR method. However, the computational time of KI is relatively high (according to Fig. 18) since its delay is much lower than that in the SHR method, but the computational time is almost similar to the SHR method.

Considering the robustness and speed of response in dealing with several simulations and experimental testing of the inrush and fault scenarios, a little higher computational burden is expected from the proposed method.

Considering the robustness and speed of response in dealing with several simulation and experimental set-up testing the inrush and fault scenarios, a little higher computational burden is expected from the proposed method.

4.8. Quantitative and qualitative comparison between the proposed method and the Hausdorff distance-based index

This section is dedicated to discussions regarding the qualitative and quantitative performance comparisons of the proposed index in this paper and the Hausdorff distance based index (HDI) [39]. Recently, authors in [39] have presented a new index based on the Hausdorff distance which could be used to distinguish internal faults, magnetizing inrush, and faults accompanied by CT saturation of the transformer. HDI basically calculates the dissimilarity of the normalized current waveform and a standard sinusoidal waveform. As stated in [39], in the case of internal fault current, the dissimilarity is very low and the index is close to 1. However, in the case of other disturbances (i.e. magnetizing inrush and faults accompanied by CT saturation of the transformer), the dissimilarity is high and the index goes toward zero [39]. The significant advantage of the HDI lies in its low computational burden and fast decision making in most cases investigated in [39]. However, the HDI requires normalized current signal, i.e., at least half cycle data is needed to find the first amplitude of the current. After that, the HDI calculation is conducted based on the data from the first quarter of the cycle. Comparing the proposed method and the HDI, the proposed index requires only the first quarter of the cycle (and in some cases even less). Moreover, during internal fault, CT deep saturation may result in distortions in the current waveforms in less than quarter of cycle. In such circumstances, reliable operation of the protective algorithm in detecting the fault scenario becomes crucial. In the following, the performance of the HDI and the proposed method is investigated for two internal fault scenarios with deep CT saturation. These two scenarios are previously discussed in subsections 4.2 and 4.5 for Y/Y and Y/D power transformers, respectively. It should be noted that in the implementation of the HDI, the threshold is chosen 0.77 [39].

As it can be seen in Figs. 19 and 20, HDI reaches above the threshold, in both cases, in less than 0.5 ms and immediately goes under the threshold due to the deep CT saturation. In other words, in the first quarter of the cycle following the fault inception, the HDI has no reliable and stable decision making. However, it can be seen in Figs. 19 and 20 that the proposed method offers reliable and stable decision making in the first quarter of the cycle following the fault inception.

5. Conclusions

Accurate, reliable, and quick discrimination of fault and magnetization inrush currents in power transformers avoids unnecessary and potentially destructive interruptions due to differential protection maloperation. Centered on the kurtosis, this paper presents new quantitative twofold indices for power transformer differential protection. Mathematically described and proven, the proposed algorithm can discriminate fault currents from inrush currents. The proposed discrimination twofold indices are designed so that it operates in the unsaturated interval of the current signals considering the decaying DC components in the fault current of the CT transient response. We also demonstrated how the parameter estimation process is accomplished in unsaturated interval, and as a result, CT saturation does not affect the performance of the proposed discrimination twofold indices. The performance of the proposed method is investigated under different inrush current scenarios without/with power transformer flux remanence, internal fault current without/with CT saturation, and also transformer energization with internal faults. It is observed that in most cases, the proposed method operates in sub-cycle, while the second harmonic restrain method needed multiple cycles for a reliable decision making. It is observed that the proposed method offers a promising margin with the selected threshold while in some cases, the second harmonic

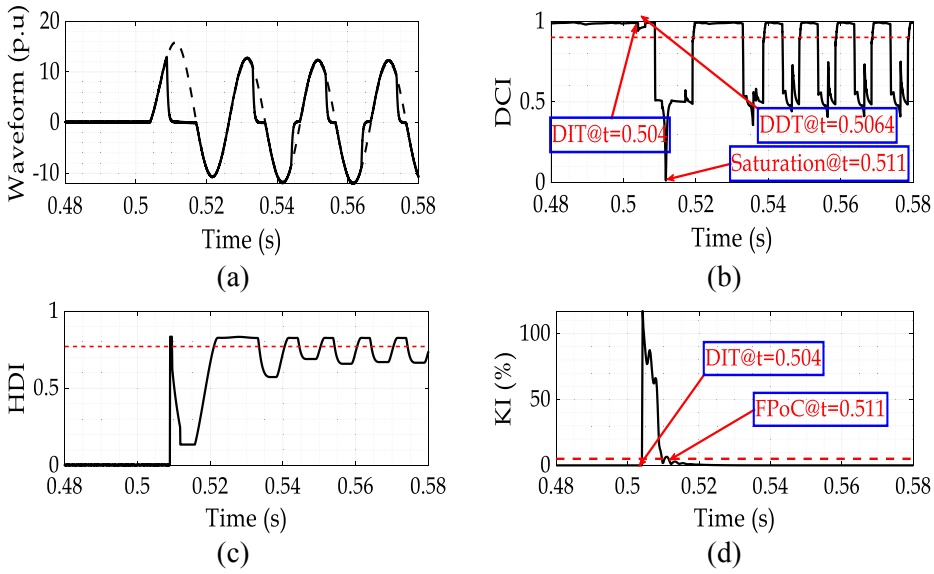

Fig. 20. Evaluating the performance of the proposed algorithm on fault current with CT saturation for Y/Δ-connected transformers: (a) current signal, (b) disturbance classification index, (c) Hausdorff distance based algorithm, (d) proposed method.

restrain method falsely violates the threshold in some samples of time, thereby compromising the required security and dependability criteria. The performance of the proposed method was tested based on the recorded experimental data. It was illustrated that the proposed method revealed a very fast response with reliable performance compared to the second harmonic restrain method. However, proposed method due to comprehensiveness has more complexity which causes relatively higher computational burden. According to the studied simulation and experimental test results, the proposed algorithm can provide a new reliable and robust basis for differential protection in power transformers.

Future work will be dedicated to relaxing the complexity of the criterion in decision making and to elevate the computational efficiency, which will simultaneously ensure reliable operation in the worst-case scenarios.

Appendix1

As proven in [3], the fundamental phasor component of (1) can be assessed utilizing well-known least squares error (LSE) technique as follows:

$$\hat{I}_x = (\hat{I}_s^T \hat{I}_s)^{-1} \hat{I}_s^T \hat{I} \tag{A1.1}$$

where,

$$\hat{I}_x = [I_1 \cos\varphi_1 \quad I_1 \sin\varphi_1 \quad I_{dc} \quad I_{CT}]^T \tag{A1.2}$$

$$\hat{I} = [i(t_1) \quad i(t_2) \quad i(t_3) \quad \cdots \quad i(t_m)]^T \tag{A1.3}$$

$$\hat{I}_s = \begin{bmatrix} \sin(2\pi f t_1) & \cos(2\pi f t_1) & e^{-t_1/\tau_{dc}} & e^{-t_1/\tau_{CT}} \\ \sin(2\pi f t_2) & \cos(2\pi f t_2) & e^{-t_2/\tau_{dc}} & e^{-t_2/\tau_{CT}} \\ \sin(2\pi f t_3) & \cos(2\pi f t_3) & e^{-t_3/\tau_{dc}} & e^{-t_3/\tau_{CT}} \\ \vdots & \vdots & \vdots & \vdots \\ \sin(2\pi f t_m) & \cos(2\pi f t_m) & e^{-t_m/\tau_{dc}} & e^{-t_m/\tau_{CT}} \end{bmatrix} \tag{A1.4}$$

where, $\hat{I}$ shows the current signal samples. Also, $\hat{I}_s$ and $\hat{I}_x$ show the matrices of known and unknown parameters, respectively. The number of current samples that is needed for solving (A1.1) is represented by subscript m and it is selected equal to 12 samples.

To evaluate (A1.1), it is necessary to assess the system time constantτ_{dc}. It is worth mentioning that the CT time constant $\tau_{CT}$is assumed known [3]. The system time constant$\tau_{dc}$is calculated as follows:

$$\tau_{dc} = \frac{-\Delta t}{\ln\left(\frac{x_2(t+\Delta t) - \lambda_{CT} x_1(t+\Delta t)}{x_2(t) - \lambda_{CT} x_1(t)}\right)} \tag{A1.5}$$

where, $x_1(t)$, $x_1(t)$, ψ_{dc}, ψ_{dc}, λ_{dc}, λ_{CT}, η and α are interim variables and calculated as follows [3]:

$$x_1(t) = I_{dc}\psi_{dc} e^{-t/\tau_{dc}} + I_{CT}\psi_{CT} e^{-t/\tau_{CT}} \tag{A1.6}$$

$$x_2(t) = I_{dc}\lambda_{dc} e^{-t/\tau_{dc}} + I_{CT}\lambda_{CT} e^{-t/\tau_{CT}} \tag{A1.7}$$

$$\psi_{dc} = 1 - \frac{\tau_{dc}^2}{\eta^2}(e^{-T_s/\tau_{dc}} - 1)^2 e^{2\alpha/\tau_{dc}} \tag{A1.8}$$

$$\psi_{CT} = 1 - \frac{\tau_{CT}^2}{\eta^2}(e^{-T_s/\tau_{CT}} - 1)^2 e^{2\alpha/\tau_{CT}} \tag{A1.9}$$

$$\lambda_{dc} = (\frac{-1}{\eta}(e^{-T_s/\tau_{dc}} - 1)e^{\alpha/\tau_{dc}})(1 - \frac{\tau_{dc}^2}{\eta^2}(e^{-T_s/\tau_{dc}} - 1)^2 e^{2\alpha/\tau_{dc}}) \tag{A1.10}$$

$$\lambda_{CT} = (\frac{-1}{\eta}(e^{-T_s/\tau_{CT}} - 1)e^{\alpha/\tau_{CT}})(1 - \frac{\tau_{CT}^2}{\eta^2}(e^{-T_s/\tau_{CT}} - 1)^2 e^{2\alpha/\tau_{CT}}) \tag{A1.11}$$

$$\eta = \frac{1}{\pi f}\sin(\pi f T_s) \tag{A1.12}$$

$$\alpha = \pi f T_s \tag{A1.13}$$

Appendix 2

In Table A2.1, the specification of the test system provided in Fig. 3 are tabulated (See Figs. A2.1 and A2.2; Table A2.2).

Table A2.1
The specification of the test system.

Component	Specifications
138 kV source	$R_+ = 7.1\ \Omega$, $L_+ = 53.99$mH $R_0 = 7.596\ \Omega$, $L_0 = 115.45$mH
13.8 kV source	$R_+ = 1.4\ \Omega$, $L_+ = 5.6$mH $R_0 = 1.498\ \Omega$, $L_0 = 11.957$mH
Power transformer	$R_1 = 0.908\ \Omega$, $L_1 = 78.51$mH $R_2 = 0.0091\ \Omega$, $L_2 = 0.7851$mH $R_c = 1.19$MΩ,
Transmission line	$R_1 = 0.3101\ \Omega$, $L_1 = 2.41$mH $C_1 = 26.8$nF, $R_0 = 0.1437\ \Omega$ $L_0 = 11.45$mH, $C_0 = 5.635$nF

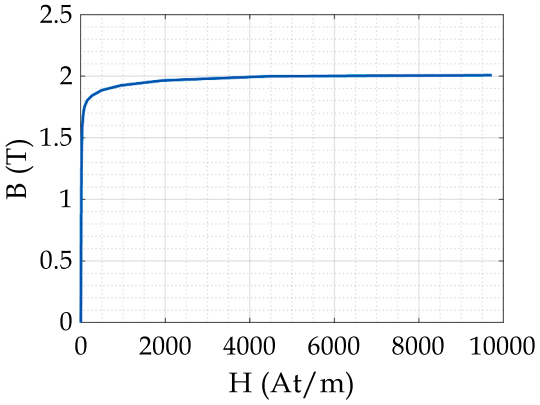

Fig. A2.1. Magnetization Curve of CTs.

Table A2.2
Specification of the CTs.

	Turn Ratio	Mean core length	Cross section area	Winding resistance	Burden
CT1	100	42.5 cm	30 mm^2	2.3 Ω	10 VA
CT2	1200	106 cm	97 mm^2	7.2 Ω	20 VA

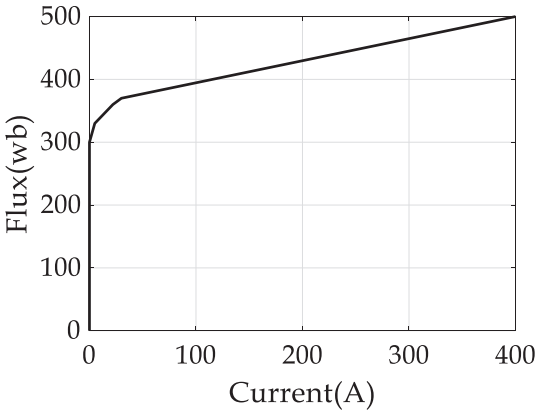

Fig. A2.2. Magnetization Curve of Transformer.

Appendix 3

List of abbreviations and symbols that are used in the paper is as follows:

CT	current transformer
DC	direct current
DCI	disturbance classification index
std	standard deviation
KI	kurtosis index
K_{SD}	kurtosis values based on the second order derivative current signal
K_{φ}	kurtosis values based on estimated phase angle
K_R	the ratio of the K_{SD} and K_{φ}
SHR	second harmonic restrain
TH1	threshold value DCI
TH2	the threshold of the KI
SHR_T	threshold on the SHR
DIT	disturbance inception time, , and
DDT	disturbance detection time
FPoC	first point of convergence
S.O	saturation occurrence
PM	Proposed Method
I_1	magnitude of the fundamental component,
I_{dc}	magnitude decaying DC offset caused by the grid
I_{CT}	magnitude decaying DC offset caused by the CT
τ_{dc}	time constant of the decaying DC offset caused by the grid
τ_{CT}	time constant of the decaying DC offset caused by the CT
φ_1	phase angle of the fundamental component
f	system frequency
i“(t)	second derivation
X	random variable
K	Kurtosis
E	Expectation
t_i	sample time
T_a	arbitrary time window
μ_a	the mean value of i“(t)
Y_i	interim coefficient
σ_a	Standard deviation corresponding to T_a

Appendix A. Supplementary data

Supplementary data to this article can be found online at https://doi.org/10.1016/j.ijepes.2020.105939.

References

[1] Mirsalim M, Masoum MAS. Application of a recursive phasor estimation method for adaptive fault component based differential protection of power transformers. IEEE Trans Ind Inf 2017;13(3):1381–92.
[2] Bagheri S, Moravej Z, Gharehpetian GB. Classification and discrimination among winding mechanical defects, internal and external electrical faults, and inrush current of transformer. IEEE Trans Ind Inf 2018;14(2):484–93.
[3] Tajdinian M, Bagheri A, Allahbakhshi M, Seifi AR. Framework for current transformer saturation detection and waveform reconstruction. IET Generation, Transmission & Distribution 2018;12(13):3167–76.
[4] Kang YC, Lim UJ, Kang SH, Crossley PA. Compensation of the distortion in the secondary current caused by saturation and remanence in a CT. IEEE Trans Power Delivery Oct. 2004;19(4):1642–9.
[5] Badrkhani F, Sanaye-Pasand M, Davarpanah M, Rezaei-Zare A, Iravani R. Compensation of the current-transformer saturation effects for digital relays. IEEE Trans Power Delivery Oct. 2011;26(4):2531–40.
[6] Hajipour E, Vakilian M, Sanaye-Pasand M. Current-transformer saturation compensation for transformer differential relays. IEEE Trans Power Delivery Oct. 2015;30(5):2293–302.
[7] Biswal Sandeep, Biswal Monalisa. Detection of current transformer saturation phenomenon for secured operation of smart power network. Electr Power Syst Res Oct. 2019;175:1–10.
[8] Delzendeh M, Kazemi Karegar H. Current Transformer Saturation Compensator by Using Negative Voltage Feedback. IEEE Trans Power Delivery 2019. https://doi.org/10.1109/TPWRD.2019.2936449.
[9] A. Bagheri, M. Allahbakhshi, H. Samet, M. Tajdinian, A. Seifi, Distinguishing

between Fault and Inrush Current in Presence of the CT Saturation: A New Method Based on Gravity Center in Time. In: 2019 IEEE International Conference on Environment and Electrical Engineering and 2019 IEEE Industrial and Commercial Power Systems Europe (EEEIC / I&CPS Europe), Genova, Italy, 2019, pp. 1-5.
[10] K. Wang, J. Tang, G. Chen, H. Hou, F. Yang, Saturation Test Under High Current for Current Transformer Detection System Based on Lab VIEW, In: 2018 China International Conference on Electricity Distribution (CICED), Tianjin, 2018, pp. 1861-1864.
[11] O. P. Mahela, H. Joshi, D. Sharma, S. Sahay, Detection of Saturation of Core of Current Transformer Using Combined Feature of Hilbert Transform and Stockwell Transform. In: 2018 IEEE 8th Power India International Conference (PIICON), Kurukshetra, India, 2018, pp. 1-6.
[12] S. Biswal, M. Biswal, Algorithm for CT Saturation Detection with the Presence of Noise, In: 2018 4th International Conference on Electrical Energy Systems (ICEES), Chennai, 2018, pp. 248-251.
[13] Erenturk K. ANFIS-based compensation algorithm for current transformer saturation effects. IEEE Trans Power Delivery Jan. 2009;24(1):195–201.
[14] Yu DC, Cummins JC, Wang Z, Yoon HJ, Kojovic LA. Correction of current transformer distorted secondary currents due to saturation using artificial neural networks. IEEE Trans Power Delivery Apr. 2001;16(2):189–94.
[15] Hong YY, Chang-Chian PC. Detection and correction of distorted current transformer current using wavelet transform and artificial intelligence. IET Gener Transm Distrib July 2008;2(4):566–75.
[16] Chothani NG, Bhalja BR. New algorithm for current transformer saturation detection and compensation based on derivatives of secondary currents and Newton's backward difference formulae. IET Gener Transm Distrib May 2014;8(5):841–50.
[17] A. Bagheri, M. Allahbakhshi, D. Behi, M. Tajdinian, Utilizing Rogowski coil for saturation detection and compensation in iron core current transformer. In: Iranian Conference on Electrical Engineering (ICEE), Tehran, 2017, pp. 1066-1071.
[18] Ji T, Shi M, Li M, Zhang L, Wu Q. Current Transformer Saturation Detection Using Morphological Gradient and Morphological Decomposition and Its Hardware Implementation. IEEE Trans Ind Electron 2017;64(6):4721–9.
[19] Roy NK, Roy Pota H. Current status and issues of concern for the integration of distributed generation into electricity networks. IEEE Syst J 2015;9(3):933–44.
[20] Jarrahi MA, Samet H, Ghanbari T. Fast Current-Only Based Fault Detection Method in Transmission Line. IEEE Syst J June 2019;13(2):1725–36.
[21] Samet H, Ghanbari T, Jarrahi MA, Ashtiani HJ. Efficient Current-Based Directional Relay Algorithm. IEEE Syst J June 2019;13(2):1262–72.
[22] Liu P, Malik OP, Chen D, et al. Improved operation of differential protection of power transformers for internal faults. IEEE Trans Power Delivery 1992;7(4):1912–9.
[23] Zhang Hao, Liu Pei, Malik OP. A new scheme for inrush identification in transformer protection. Electr Power Syst Res 2002;63(2):81–6.
[24] Zheng T, Huang T, Ma Y, Zhang Z, Liu L. Histogram-based method to avoid maloperation of transformer differential protection due to current-transformer saturation under external faults. IEEE Trans Power Delivery 2018;33(2):610–9.
[25] Ali E, Helal A, Desouki H, Shebl K, Abdelkader S, Malik OP. Power transformer differential protection using current and voltage ratios. Electr Power Syst Res 2018;154:140–50.
[26] A. G. Phadke, J. S. Thorp, A new computer-based flux-restrained curretn-differential relay for power transformer protection. In: IEEE Trans. Power Appar. Syst. PAS-102, pp. 3624–3629, 1983.
[27] S. Member, A novel transformer protection method based on the ratio of voltage and fluxional differential current. In: Proceedings of IEEE Transmission and Distribution Conference and Exposition, pp. 342–347, 2003.
[28] Kang YC, Lee BE, Kang SH. Transformer protection relay based on the induced voltages. Int J Electr Power Energy Syst 2007;29:281–9.
[29] Baoming G, Almeida AT, Qionglin Z, Xiangheng W. An equivalent instantaneous inductance-based technique for discrimination between inrush current and internal faults in power transformers. IEEE Trans Power Delivery October 2005;20(4):2473–82.
[30] Tripathy M, Maheshwari RP, Verma HK. Power transformer differential protection based on optimal probabilistic neural network. IEEE Trans Power Delivery 2010;25(1):102–12.
[31] Perez L, Flechsig A, Meador J, Obradovic Z. Training an artificial neural network to discriminate between magnetizing inrush and internal faults. IEEE Trans Power Delivery Jan. 1994;9(1):434–41.
[32] Yazdani-Asrami M, Taghipour-Gorjikolaie M, Razavi SM, Gholamian SA. A novel intelligent protection system for power transformers considering possible electrical faults, inrush current, ct saturation and over-excitation. International Journal of Electric Power and Energy Systems 2015;64:1129–40.
[33] Rahmati A, Sanaye-Pasand M. Protection of power transformer using multi criteria decision-making. International Journal of Electric Power and Energy Systems 2015;68:294–303.
[34] Shin MC, Park CW, Kim JH. Fuzzy logic-based relaying for large power transformer protection. IEEE Trans Power Delivery 2018;18(3):718–24.
[35] Guillén D, Esponda H, Vázquez E, Idárraga-Ospina G. Algorithm for transformer differential protection based on wavelet correlation modes. IET Gener Transm Distrib 2016;10:2871–9.
[36] Medeiros RP, Costa FB, Silva K. Power transformer differential protection using the boundary discrete wavelet transform. IEEE Trans Power Delivery Oct. 2016;31(5):2083–95.
[37] Marques JP, Lazaro C, Morais AP, Cardoso G. A reliable setting-free technique for power transformer protection based on wavelet transform. Electr Power Syst Res Sept. 2018;162:161–8.
[38] Zhang LL, Wua QH, Ji TY, et al. Identification of inrush currents in power transformers based on higher-order statistics. Electr Power Syst Res 2017;9:146–61.
[39] Weng H, Wang S, Lin X, Li Z, Huang J. A novel criterion applicable to transformer differential protection based on waveform sinusoidal similarity identification. Int J Electr Power Energy Syst 2019;105:305–14.
[40] Weng Hanli, Wang Sheng, Wan Yi, Lin Xiangning, Li Zhenxing, Huang Jingguang. Discrete Fréchet distance algorithm based criterion of transformer differential protection with the immunity to saturation of current transformer. Int J Electr Power Energy Syst 2020;115:105–14.
[41] Tajdinian M, Jahromi MZ, Mohseni K, Kouhsari SM. An analytical approach for removal of decaying DC component considering frequency deviation. Electr Power Syst Res 2016;130:208–19.
[42] Tajdinian M, Seifi AR, Allahbakhshi M. Half-cycle method for exponentially DC components elimination applicable in phasor estimation. IET Sci Meas Technol 2017;11(8):1032–42.
[43] Allahbakhshi M, Tajdinian M, Seifi AR, Zareian Jahromi M, Bagheri A. Hybrid approach for immunization of DFT-based phasor estimation method against decaying DC components. IET Sci Meas Technol 2018;13(2):238–46.
[44] Mendel JM. Tutorial on higher-order statistics (spectra) in signal processing and system theory: theoretical results and some applications. Proceedings of IEEE 1991;79(3):278–305.
[45] Brahma SM, De Leon PL, Kavasseri RG. Investigating the Option of Removing the Antialiasing Filter From Digital Relays. IEEE Trans Power Delivery Oct. 2009;24(4):1864–8.
[46] S. Das, Possibility of phasor estimation in digital relays without using anti-aliasing filter and very high sampling rates. In: 2016 Power Systems Computation Conference (PSCC), Genoa, 2016, pp. 1-7.